Al-Nahrain Journal for Engineering Sciences **NJES** 28(2)205-211, 2025
http://doi.org/10.29194/NJES.28020205

The Effect of Wind Loading on the Growth of Crack Propagation in Aircraft Wing

Shahad Nashat Subhi[1], Fathi Al-shamma [2*]

Authors affiliations:
1) Mechanical Engineering Department, College of Engineering, University of Baghdad, Iraq.
shahad.sobhi2303@coeng.uobaghdad.edu.iq

2*) Mechanical Engineering Department, College of Engineering, University of Baghdad, Iraq.
fathi_alshamma@coeng.uobaghdad.edu.iq

Paper History:

Received: 30th Aug. 2024

Revised: 4th Oct. 2024

Accepted: 8th Nov. 2024

Abstract

Throughout the flight, aircraft wings continuously struggle against various forces: the forward thrust from the engine, the drag pulling them backward, and sudden turbulence from storms. In contrast, these forces are essential for maintaining aircraft stability. With time, the cyclic stresses can result in the formation and propagation of minuscule cracks in the wings. Cracks growing on the aircraft wing surface manufactured from alloy AL7075-T6, have been investigated when subjected to non-preoperational multi-axial cyclic loading. The results have been evaluated using two methods, numerical simulations and theoretical calculation to evaluate dynamic crack propagation crack growth per cycle (da/dN) at angles of attack 5° and 10°. The results showed that the dynamic crack propagation increases with an increase in the crack length. It was found that the values of the dynamic crack propagation rate at the angle of attack 5^0 are smaller than the values at the angle of attack 10^0.

Keywords: Dynamic crack propagation, Computational fluid dynamics, Non-preoperational multi-axial cyclic load, AL7075-T6 alloy, Angle of attack (AOA).

تأثير أحمال الرياح على نمو التشققات في أجنحة الطائرات

شهد نشأت صبحي ، فتحي الشماع

الخلاصة:

طوال الرحلة، تكافح أجنحة الطائرات باستمرار ضد قوى مختلفة: الدفع الأمامي من المحرك، والسحب الذي يسحبها للخلف، والاضطرابات المفاجئة من العواصف. على النقيض من ذلك، فإن هذه القوى ضرورية للحفاظ على استقرار الطائرة. مع مرور الوقت، يمكن أن تؤدي الاجهادات المتكررة إلى تكوين وانتشار الشقوق الصغيرة في الأجنحة. تم التحقيق في الشقوق التي تنمو على سطح جناح الطائرة المصنوع من سبيكة المنيوم 7075-T6، عند تعرضها لتحميل دوري متعدد المحاور غير متناسب. تم تقييم النتائج باستخدام طريقتين، المحاكاة العددية والحساب النظري لتقييم نمو الشقوق الديناميكي لكل دورة (da / dN) عند زوايا هجوم 5° و 10°. أظهرت النتائج أن انتشار الشقوق الديناميكية يزداد مع زيادة طول الشق. حيث وجد أن قيم معدل انتشار الشقوق الديناميكية عند زاوية الهجوم 5° أصغر من القيم عند زاوية الهجوم 10°.

1. Introduction

Modern civilian and military aircraft are engineering marvels made up of five primary components: the fuselage, engines, landing gear, tail assembly, and wings. However, they face significant challenges from extreme weather conditions. Wings, in particular, are highly susceptible to damage due to their critical role in generating lift and maintaining stability.

The effect of wind on crack propagation in aircraft wings involves complex interactions between aerodynamic forces, structural dynamics, and material properties. [2]

The detailed exploration of the key factors:

1. **Aerodynamic Forces:**
   Lift, Drag, Pressure Distribution, Turbulence and Gusts.
2. **Structural Fatigue and Crack Propagation:** Cyclic Loading, Stress Concentration, and Crack Growth Mechanisms
3. **Material Behavior and Fracture Mechanics:** Fatigue Crack Growth Rate, Fracture Toughness, and Environmental Effects).
4. **Detection and Monitoring**:
   Non-Destructive Testing and Structural Health Monitoring.
5. **Mitigation Strategies**:
   Design Optimization, Material Selection, and Maintenance and Inspection

NJES is an **open access Journal** with **ISSN 2521-9154** and **eISSN 2521-9162**

The propagation of cracks in aircraft wings due to wind effects is a multifaceted problem that requires a comprehensive understanding of aerodynamic forces, structural dynamics, material behavior, and advanced monitoring techniques. Addressing these factors through design optimization, material selection, and regular maintenance is essential for ensuring the safety and longevity of aircraft.

2. Numerical simulations

Numerical analysis is a branch of mathematics focused on developing techniques to find approximate solutions to problems that are mathematically formulated but cannot be solved exactly with analytical methods. Such problems frequently occur in scientific computing, engineering, and other fields that depend on mathematical models. In this study, ANSYS CFD was utilized for airfoil analysis, leveraging its robust capabilities for simulating airflow. This makes it an invaluable tool for examining the behavior of airfoils, which are crucial components of aircraft design and play a significant role in achieving desired aerodynamic performance. CFD was used to determine lift, drag, pressure distribution, and center of pressure. This pressure distribution data was then used to calculate equivalent stress, which is necessary to achieve the desired outcomes [3].

Finally, ANSYS engineering simulation software was used to obtain numerical results by inputting the parameters of Paris's law (including the constants ccc and mmm), ΔK (change in stress intensity factor), and $\partial a/\partial N$ (crack growth per cycle) [4].

2.1. Computational fluid dynamics

It plays a crucial role in designing aerodynamically efficient airplanes and optimizing energy production.

By utilizing numerical analysis and data structures to simulate fluid flow, this branch of fluid mechanics proves indispensable across various industries.

CFD, which stands for Computational Fluid Dynamics, is a powerful tool for simulating the flow of fluids around objects, such as airfoils. Airfoils, which are wing-shaped structures found in airplanes, helicopters, wind turbines, and other applications, are analyzed at various angles of attack [5].

In this paper, the aircraft model will be examined at angles of attack of 5° and 10°. The angle of attack will be 5° during cruising speed, while it will increase to 10° for takeoff and landing. Maintaining the correct angle of attack is crucial during landing, particularly near the runway during the flare maneuver. This precise angle ensures an accurate touchdown and prevents stalling, a dangerous situation that requires immediate corrective action [6].

By employing CFD, engineers can predict the aerodynamic performance of an airfoil, including its lift, drag, and pressure distribution. This information is vital for designing efficient and safe airfoils and for studying the growth of cracks.[7].

2.1.1.Computational method for predicting fluid flow characteristics

To accurately model wind pressure on the wing, a control volume was created (Fig. 1) to encompass the air surrounding the wing model. The wing's volume was then subtracted from this control volume using SOLIDWORKS, ensuring that all wing surfaces experienced realistic wind pressure during the analysis. The model was subsequently imported into ANSYS Workbench for further investigation. Standard air properties were applied: a density of 1.225 kg/m³, a temperature of 288.2 K, and a viscosity of 1.7889×10^-5 kg·m/s. The wing geometry was discretized using a pre-existing mesh from the ANSYS library, which included 5,257,559 fluid tetrahedron elements and 1,480,217 nodes. Airflow entered the control volume at 114 m/s through an inlet face near the leading edge of the wingtip, while the opposite face served as the outlet with zero gauge pressure.

The CFD analysis provided data on lift, drag, center of pressure, and the air pressure distribution across the wing surfaces. [8].

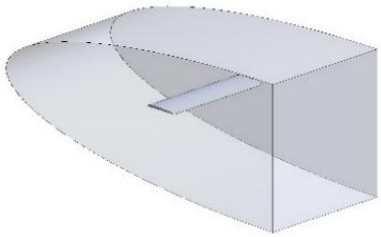

Figure (1): Manage fluid volume utilizing a wing enclosed within (Source: Authors).

The CFD analysis aimed to evaluate how air pressure is distributed across the wing surfaces. Boundary conditions for a wing in CFD simulations include [Inlet boundary condition: velocity inlet (variable), Outlet Boundary Condition: pressure outlet (zero), airfoil boundary condition: wall (no-slip condition)]. A relationship between the wing's shape and the pressure distribution was noted (Fig. 2), with higher pressure occurring near the leading edge towards the wingtip. This explains why, at cruising speed with an angle of attack of 5°, the maximum pressure of 7.736 kPa was concentrated near the fixed end.

During takeoff and landing, as the angle of attack increases to 10° (Fig. 3), the pressure distribution shifts, with the maximum pressure of 7.664 kPa now concentrated at the wingtip, the point furthest from the fixed end.

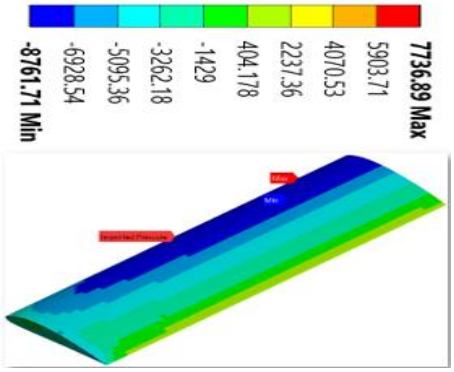

Figure (2): Pressure distribution on the wing within the designated volume at AOA 5°

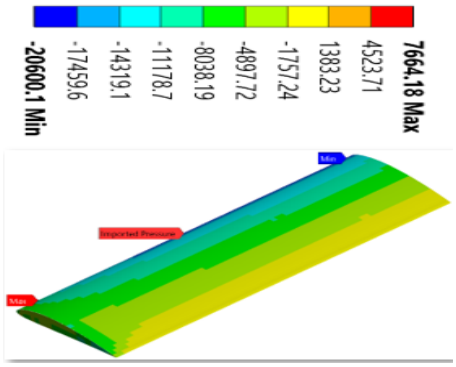

Figure (3): Pressure distribution on the wing within the designated volume at AOA 10°

2.1.2. Analysis of structures under static loads

The CFD pressure data was used to inform the subsequent static structural analysis in ANSYS of a simplified cantilever wing model subjected to varying wind loads. Stress variations across the structure were examined through two separate simulations, using the material properties outlined in Table 1, which correspond to alloy AL7075-T6. [9]

Table (1): Material Properties of alloy AL7075-T7.

NO.	MATERIAL AL7075-T6	
1	Density	2780 kg/m³
2	Coefficient of Thermal Expansion	2.3×10^{-05} / °C
3	Reference Temperature	21 °C
4	Young's Modulus	71.5 GPa
5	Poisson's Ratio	0.33
6	Bulk Modulus	71 GPa
7	Shear Modulus	28 GPa
8	Tensile Yield Strength	503 MPa
9	Compressive Yield Strength	503 MPa
10	Tensile Ultimate Strength	570MPa

To evaluate the stress distribution within the wing structure, the computer model was segmented into 5,257,567 small tetrahedral elements, chosen from the ANSYS software library. The number of elements was determined by focusing on regions with the highest stress concentrations. Pressure distribution data obtained from a separate fluid flow analysis, along with the resulting lift and drag forces on the wing surface, were applied to the meshed model. Key stress indicators, such as equivalent Von Mises stress, maximum principal stress, and maximum shear stress, were then analyzed.

A comprehensive stress value for the wing was determined, considering all potential stress factors that could lead to deformation or failure. As anticipated, the equivalent stress was highest at the wingtip, reaching 26.533 MPa at a 5° angle of attack and 39.776 MPa at a 10° angle of attack. This increase was attributed to the combined effects of maximum wing pressure in that area and the influence of drag force (Fig. 4). The stress distribution across the wing was primarily tensile.

The analysis further highlighted the shear stress distribution along the wing (Fig. 5), showing that the highest shear stress occurred at the leading edge. At a 5° angle of attack, the maximum shear stress reached 14.999 MPa, increasing to 22.46 MPa at a 10° angle of attack.

3. Theoretical Analysis

Wing model constructed from AL7075-T6 alloy. The model's dimensions are 300 mm × 60 mm × 2 mm, and an elliptical crack measuring 1 mm × 5 mm will be introduced at one end using a wire-cutting machine. The crack will be positioned 30 mm from the edge where the shear load will be applied.

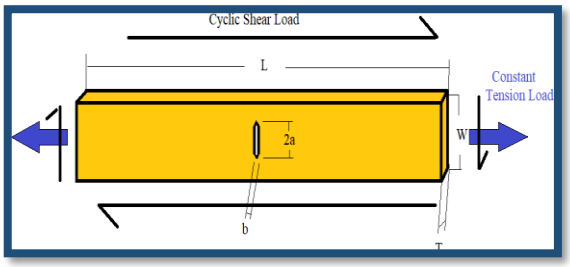

Figure (6): Multiaxial cyclic loading with thin plate.

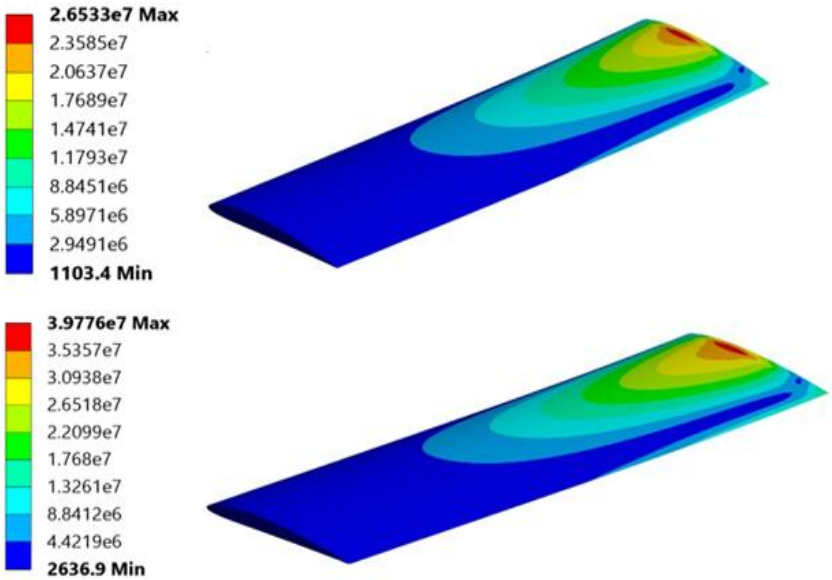

Figure (4): Equivalent von Mises stress at 5° and 10°

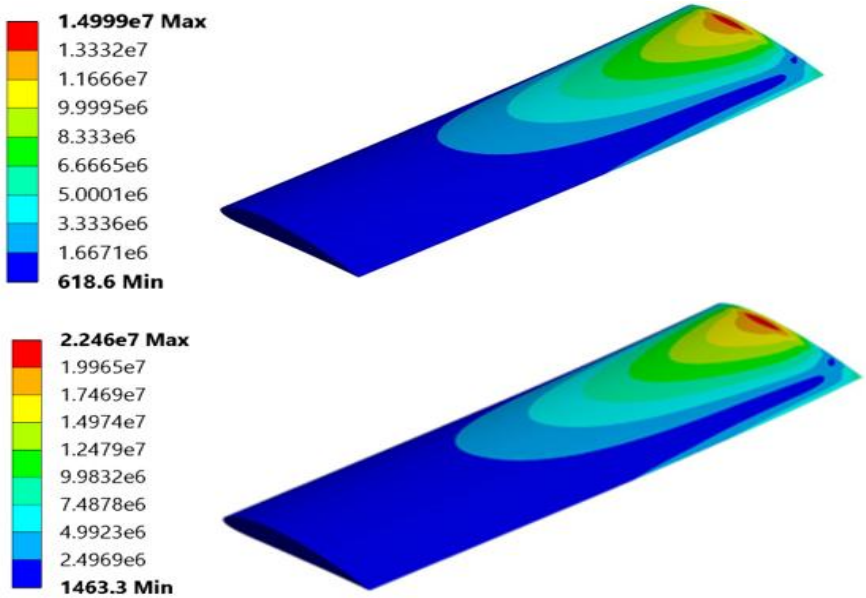

Figure (5): Maximum shear stress at 5° and 10°

This investigation will explore the Griffith energy criterion, which examines the energy dynamics in brittle materials, such as glass, containing a single prominent crack running through it. The study will focus on a large, flat specimen of such material under the influence of external forces.

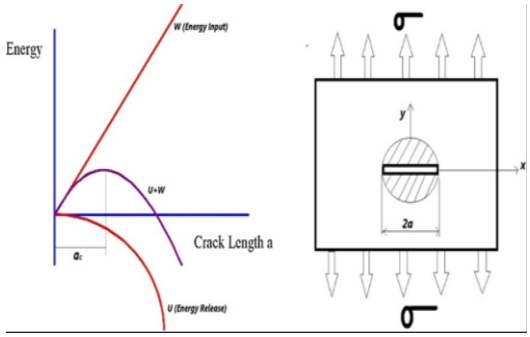

Figure (7): The relationship between energy input and release as a function of crack length. a material under constant pressure (σ) and experiencing repeated twisting forces (τ).[10]

This results in a distinct quantity of energy stored per unit volume, which can be determined using the following equation. [10]: -

$$U_0 = \frac{1}{2}\left(\sigma_X\varepsilon_X + \sigma_y\varepsilon_y + \sigma_z\varepsilon_z + \tau_{Xy}\gamma_{Xy} + \tau_{yz}\gamma_{yz} + \tau_{Xz}\gamma_{Xz}\right) \quad \dots\dots(1)$$

$$U_0 = \frac{1}{2E}\left(\sigma_X + \sigma_y + \sigma_z\right)^2 - \frac{2(1-\nu)}{E}\left(\sigma_X\sigma_y + \sigma_y\,\sigma_z + \sigma_z\sigma_x - \left(\tau_{Xy}{}^2 + \tau_{yz}{}^2 + \tau_{Xz}{}^2\right)\right) \quad \dots\dots(2)$$

$$U_0 = \frac{\sigma^2}{2E} + \frac{2(1+\nu)}{E}\left(\tau\,\sin\left(\frac{\omega t}{2}\right)\right)^2 \quad \dots\dots(3)$$

$$U_0 = \left(\frac{\sigma^2}{2E} + \frac{2(1+\nu)}{E}\left(\tau\,\sin\left(\frac{\omega t}{2}\right)\right)^2\right)\left(\pi a^2 \times \frac{h}{h}\right) = \left(\frac{\sigma^2}{2E} + \frac{2(1+\nu)}{E}\left(\tau\,\sin\left(\frac{\omega t}{2}\right)\right)^2\right)\pi a^2 \quad \dots\dots(4)$$

1- The equation for the energy released per unit thickness is:[10]

$$\frac{\delta U}{\delta a} = \frac{\delta W}{\delta a} \quad \dots\dots(5)$$

2- Fracture occurs when the energy release rate reaches its maximum value [10]: -

$$G = \frac{\partial U}{\partial a} = \left(\frac{\sigma^2}{2E} + \frac{2(1+\nu)}{E}\left(\tau\,\sin\left(\frac{\omega t}{2}\right)\right)^2\right)\frac{\pi a^2}{2} \quad \dots\dots(6)$$

The additional energy resulting from an unstable fracture can be described as:[11]

$$U_e = \int_{a_0}^{a_i}(G - R)\,da \quad \dots\dots(7)$$

$$= -R\,(a_i - a_0) + \int_{a_0}^{a_i}\left(\frac{\sigma^2}{2E} + \frac{2(1+\nu)}{E}\left(\tau\,\sin\left(\frac{\omega t}{2}\right)\right)^2\right)\frac{\pi a}{2}da \quad \dots\dots(8)$$

For R $= \left(\frac{\sigma^2}{2E} + \frac{2(1+\nu)}{E}\left(\tau\,\sin\left(\frac{\omega t}{2}\right)\right)^2\right)\frac{\pi a_i}{2}$ $\dots\dots(9)$

Substituting Eq. (5) in Eq. (4) gives:[11]

$$U_e = \left(\frac{\sigma^2}{2E} + \frac{2(1+\nu)}{E}\left(\tau\,\sin\left(\frac{\omega t}{2}\right)\right)^2\right)\frac{\pi a_0}{2(a_i - a_0)} + \frac{\left(\frac{\sigma^2}{2E} + \frac{2(1+\nu)}{E}\left(\tau\,\sin\left(\frac{\omega t}{2}\right)\right)^2\right)\pi}{4({a_i}^2 - {a_0}^2)} \quad \dots\dots(10)$$

$$U_e = \frac{\left(\frac{\sigma^2}{2E} + \frac{2(1+\nu)}{E}\left(\tau\,\sin\left(\frac{\omega t}{2}\right)\right)^2\right)\pi}{4({a_i}^2 - {a_0}^2)} \quad \dots\dots(11)$$

To ascertain the widening of a crack (kinetic opening displacement) in a thin plate subjected to diverse forces in multiple directions (multi-axial loading), engineers employ the concept of "effective stress." This concept essentially simplifies the intricate interaction of forces into a single, equivalent force acting in a singular direction. The equation provided below aids in computing this effective stress. [12]: -

$$\sigma_{eff} = \frac{1}{\sqrt{2}}\sqrt{\sigma^2 + \left(\tau\,\sin\left(\frac{\omega t}{2}\right)\right)^2} \quad \dots\dots(12)$$

The concept of 'effective stress' is effective in situations involving two types of forces acting in multiple directions (non-proportional multi-axial stress). One force remains constant (such as σ in this study), akin to exerting upward pressure on an object. The other force changes direction cyclically (cycling stress, like τ). In such cases, the effective stress aids in estimating the vertical displacement of the crack (vertical displacement, v). The equation below illustrates this calculation. [11]: -

$$V = \frac{2\sigma_{eff}}{E}\sqrt{a^2 - x^2} \quad \dots\dots(13)$$

Since x is a function of (a) it can be expressed as x =Ca where 0 < C < 1 then:[13]

$$V = \frac{2\sigma_{eff}}{E}\sqrt{a^2(1-C^2)} \quad = C_1 \frac{\sigma_{eff}\, a}{E} \quad \text{……(14)}$$

Where $C_1 = 2\sqrt{(1-C^2)}$

Therefore, as the crack propagates, the displacement (v) will change over time and become:[11]

$$\frac{\partial V}{\partial t} = \frac{C_1}{E}\frac{\partial(\sigma_{eff}\, a)}{\partial t} \quad \text{……(15)}$$

$$\frac{\partial V}{\partial t} = \frac{C_1}{E}\left(\frac{\partial \sigma_{eff}}{\partial t} a + \frac{\partial a}{\partial t}\sigma_{eff}\right) \quad \text{……(16)}$$

$$\frac{\partial \sigma_{eff}}{\partial t} = \partial \frac{\left(\frac{1}{\sqrt{2}}\sqrt{\sigma^2 + \left(\left(\tau \sin\left(\frac{\omega t}{2}\right)\right)^2\right)}\right)}{\partial t} \quad \text{……(17)}$$

$$\frac{\partial V}{\partial t} = \frac{1}{\sqrt{2}}\left(\sigma^2 + \left(\tau \sin\left(\frac{\omega t}{2}\right)\right)^2\right)^{-\frac{1}{2}} \tau^2 \omega \sin\left(\frac{\omega t}{2}\right)\cos\left(\frac{\omega t}{2}\right) \quad \text{……(18)}$$

$$\frac{\partial V}{\partial t} = \frac{\omega \tau^2 \sin \omega t}{2\sqrt{2}\sqrt{\sigma^2 + \left(\tau \sin\left(\frac{\omega t}{2}\right)\right)^2}} \quad \text{……(19)}$$

Based on the dynamic conditions of crack growth, the kinetic energy associated with the crack's displacement is [11]: -

$$T = \frac{1}{2}\rho * Area * V^{0^2} \quad \text{……(20)}$$

$$T = \frac{1}{2}\rho \int\int \left(\frac{\partial V}{\partial t}\right)^2 dxdy \quad \text{…… (21)}$$

$$T = \frac{1}{2}\rho\frac{1}{E^2}\left[\left(\frac{\omega \tau^2 \sin \omega t}{2\sqrt{2}\sqrt{\sigma^2 + \left(\tau \sin\left(\frac{\omega t}{2}\right)\right)^2}} a\right) \backslash \left(\frac{\partial a}{\partial t}\frac{1}{\sqrt{2}}\sqrt{\sigma^2 + \left(\tau \sin\left(\frac{\omega t}{2}\right)\right)^2}\right)\right]^2 \int\int C_1{}^2\, dxdy$$

……………………………………………(22)

In a semi-infinite plate, it is found experimentally that the integral of $C_1{}^2$ is equal to ka^2 thus Eq. (22) could be written as [11]:

$$T = ka^2\frac{1}{2}\rho\frac{1}{E^2}\left[\left(\frac{\omega \tau^2 \sin \omega t}{2\sqrt{2}\sqrt{\sigma^2 + \left(\tau \sin\left(\frac{\omega t}{2}\right)\right)^2}} a\right) + \left(\frac{\partial a}{\partial t}\frac{1}{\sqrt{2}}\sqrt{\sigma^2 + \left(\tau \sin\left(\frac{\omega t}{2}\right)\right)^2}\right)\right]^2 \quad \text{……(23)}$$

The critical crack length at which the crack becomes unstable and starts to grow is reached when the strain energy Ue equals or exceeds the kinetic energy T. From Equations (11) and (18):

$$\frac{\left(\frac{\sigma^2}{2E} + \frac{2(1+v)}{E}\left(\tau \sin\left(\frac{\omega t}{2}\right)\right)^2\right)\pi}{4(a_i{}^2 - a_0{}^2)} = ka^2\frac{1}{2}\rho\frac{1}{E^2}\left[\left(\frac{\omega \tau^2 \sin \omega t}{2\sqrt{2}\sqrt{\sigma^2 + \left(\tau \sin\left(\frac{\omega t}{2}\right)\right)^2}} a\right) + \left(\frac{\partial a}{\partial t}\frac{1}{\sqrt{2}}\sqrt{\sigma^2 + \left(\tau \sin\left(\frac{\omega t}{2}\right)\right)^2}\right)\right]^2 \quad \text{……(24)}$$

$$= ka_i{}^2\frac{1}{2}\rho\frac{1}{E^2}\left[\left(\frac{\omega \tau^2 \sin \omega t}{2\sqrt{2}\sqrt{\sigma^2 + \left(\tau \sin\left(\frac{\omega t}{2}\right)\right)^2}} a_i\right) + \left(\frac{\partial a}{\partial t}\frac{1}{\sqrt{2}}\sqrt{\sigma^2 + \left(\tau \sin\left(\frac{\omega t}{2}\right)\right)^2}\right)\right]^2 \quad \text{……(25)}$$

Where (a_i) represents the crack length at which excess energy is released. By utilizing a MATLAB program and applying the Newton-Raphson method, from Eq. (19) it could be calculated the velocity of the crack growth $\frac{\partial a}{\partial t}$ for each time required to reach the crack length a_i. Also, the value of the limit value $\frac{\pi}{k}$ for $a_i >> a_0$ is found to be less than unity. To verify the theoretical results, the principal stresses for the element under non-proportional multiaxial cyclic loading can be calculated as [12]:

$$\sigma_{1.2} = \frac{\sigma_x + \sigma_y}{2} \pm \sqrt{\left(\frac{\sigma_x - \sigma_y}{2}\right)^2 + \tau_{xy}{}^2} \quad \text{……(26)}$$

For this study, the principal stresses can be expressed as:

$$\sigma_{1.2} = \frac{\sigma}{2} \pm \sqrt{\left(\frac{\sigma}{2}\right)^2 + \left(\tau_{xy}{}^2 \sin\left(\frac{\omega t}{2}\right)\right)^2} \quad \text{……(27)}$$

The angle of the plane of principal stresses relative to the horizontal axis can be represented as:[12]

$$\tan 2\theta_p = \frac{2\tau_{xy}}{\sigma_x - \sigma_y} \quad \text{……(28)}$$

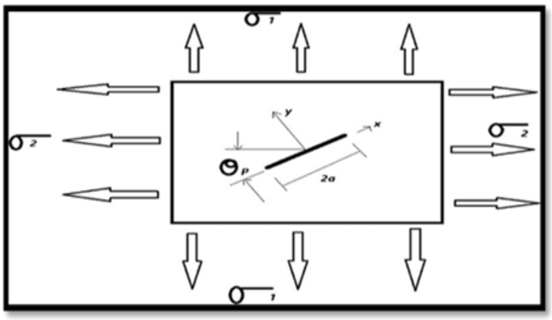

Figure (8): A crack subjected to an in-plane biaxial load (as represented in our case study**)** [10]

Which can be represented for our case of study as [10]:

$$\tan 2\theta_p = \frac{2\left(\tau_{xy}\sin\left(\frac{\omega t}{2}\right)\right)}{\sigma} \quad \text{……(29)}$$

From Equation (29), it can be demonstrated that the angle of inclination of the principal plane concerning the horizontal axis varies with the value of ωt. Given that the crack in the plate is aligned with the y-axis, it can be represented as being inclined at an angle θp with the direction of the principal stresses, as shown in Fig. 3. Consequently, the stress intensity factors for modes I and II can be expressed as follows: If $\sigma_2 = \alpha\sigma_1$, where σ_2 is always a compressive stress according to the Mohr circle for our study:[14]

$$K_I = \frac{\sigma_1\sqrt{\pi a}}{2}\{(1+\alpha) + (1-\alpha)\cos 2\theta_p\} \quad \text{……(30)}$$

$$K_{II} = \frac{\sigma_1\sqrt{\pi a}}{2}\{(1-\alpha)\sin 2\theta_p\} \quad \text{……(31)}$$

Then $K_I = K_{Imax} - K_{Imin}$ where K_{Imax} is depend on the value of σ_{1max} when sin ωt = 1 and σ_{1min} when sin ωt = 0 Also K_{II} is depend on

σ_{1max} and σ_{1min} then the mixed mode of I and II give: [14]

$$\Delta K_{eq} = \left[\left[\Delta K_I{}^4 + 8\Delta K_{II}{}^4\right]\right]^{0.25} \quad \ldots\ldots(32)$$

Crack growth can be determined using Paris's law as follows:[15]

$$\frac{\partial a}{\partial N} = C\left(\Delta K_{eq}\right)^m \quad \ldots\ldots(33)$$

The experimental measurement of $\frac{\partial a}{\partial N}$ was conducted, and C and m were determined for the current loading condition by plotting the logarithm of $\frac{\partial a}{\partial N}$ against the logarithm of ΔKeq.

The slope of the line represents m while C can be obtained from the intersection of the line with the logarithm of ∂a/∂N. In the linear region, the following equation can be utilized to determine the parameters C and m employing the equation:

$$\text{Log}\left(\frac{\partial a}{\partial N}\right) = \text{m} * \log(\Delta\text{K}) + \log \text{c}$$

4. Result and discussion

The results depicted in Figures (9 and 10), which illustrate the relationship between crack length (a) and the number of cycles (N), were obtained through ANSYS simulations and theoretical solutions. analyzed observations from the figures:

1. Crack Growth Behavior:

- For **AOA 5°**: The crack grows steadily and exhibits a gradual increase in length over time. The crack length starts at approximately 5 mm and progresses to around 12 mm after 800,000 cycles. The growth appears relatively linear with a mild increase in the rate of growth toward the higher number of cycles.
- For **AOA 10°**: The crack grows much faster than at AOA 5°. The crack length starts at a similar point (5 mm) but rapidly increases to around 12 mm in just under 200,000 cycles, indicating a much more aggressive propagation rate at this higher angle of attack.

2. Influence of AOA:

- **Higher AOA (10°)** causes significantly faster crack propagation compared to **lower AOA (5°)**. This result is consistent with the idea that higher angles of attack result in greater stress and strain on the wing, leading to a more rapid crack growth due to the increased loads experienced by the structure.

3. Fatigue Life:

- At AOA 5°, the fatigue life of the material is much longer, with cracks taking many more cycles to reach the same length compared to AOA 10°. This suggests that operating at lower angles of attack would prolong the fatigue life of the wing structure, as the crack growth rate is much slower.
- AOA 10° shows a drastic reduction in fatigue life, indicating that the structure could fail prematurely if subjected to higher angles of attack for extended periods.

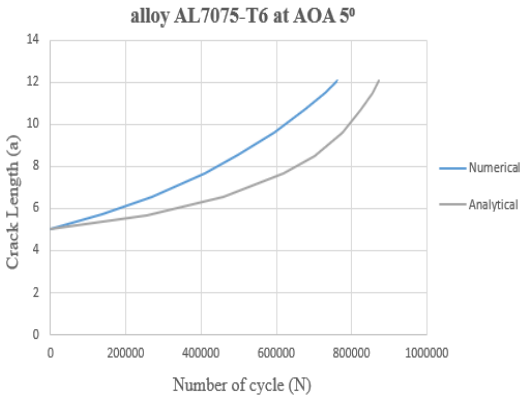

Figure (9): Crack length a (mm) vs. no. of cycles N for alloy AL7075-T6 at AOA5°

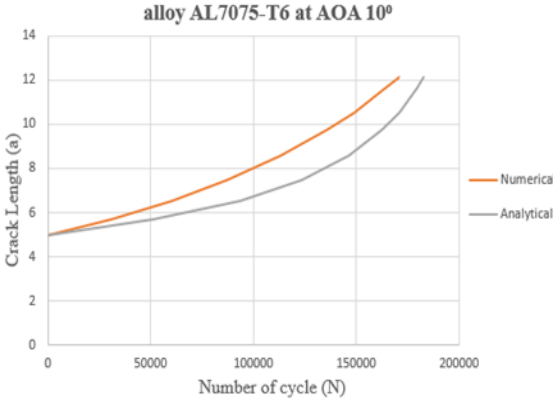

Figure (10): Crack length a (mm) vs. no. of cycles N for alloy AL7075-T6 at AOA 10°

Additionally, Figures (11 and 12) present the contour near the final stage for AL7075-T6 at angles of attack (AOA) of 5° and 10°, as determined from numerical simulations. In the final stage, the fracture crack angle (θc) is approximately 23° at AOA 5° and increases to around 26° AOA 10°.

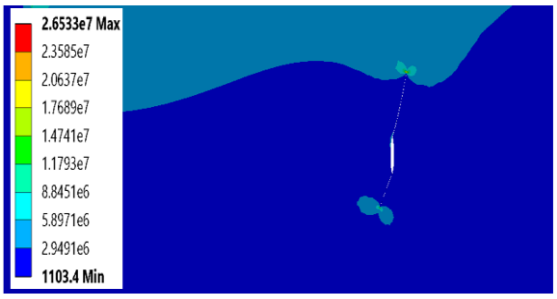

Figure (11): Near to final stage contour for alloy AL7075-T6 at AOA 5o

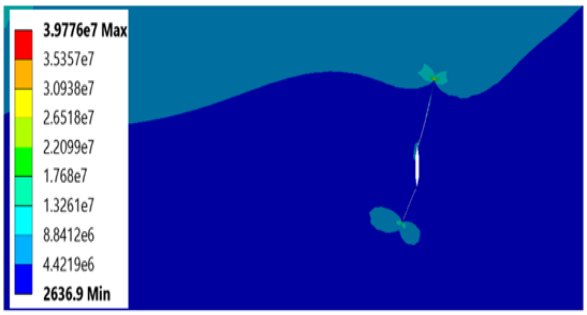

Figure (12): Near to final stage contour for alloy AL7075-T6 at AOA 10°

5. Conclusion

The results highlight the critical impact of the angle of attack on the fatigue crack propagation in alloy AL7075-T6. While the wing material can withstand a substantial number of cycles at lower AOA, the crack propagation rate increases significantly at higher AOA, leading to a shorter fatigue life. This has important implications for aircraft design and operation, particularly in ensuring that wings are not subjected to excessively high AOA for extended durations to avoid rapid crack growth and possible failure.

6. Reference

[1] S. S. T. Yau and N. Recho, "*Crack Growth and Fatigue*". Springer, 2019. DOI: 10.1007/978-3-030-26604-4

[2] Federal Aviation Administration (FAA), "*Pilot's Handbook of Aeronautical Knowledge*", FAA-H-8083-25B, Scientific Reports, 2016. DOI: 10.31236/osf.io/8xq7z

[3] J. B. Kodman, B. Singh, and M. Murugaiah, "A comprehensive survey of open-source tools for computational fluid dynamics analyses," *J. Adv. Res. Fluid Mech. Therm. Sci.*, vol. 119, no. 2, pp. 123–148, 2024. DOI: 10.37934/arfmts.119.2.123148

[4] A. Sedmak, "Fatigue crack growth simulation by extended finite element method: A review of case studies," *Fatigue Fract. Eng. Mater. Struct.*, vol. 47, no. 6, pp. 1819–1855, 2024. DOI: 10.1111/ffe.14277

[5] S. Kandwal and S. Singh, "Computational fluid dynamic study of fluid flow and aerodynamic forces on an airfoil," *Int. J. Eng. Res. Technol.*, vol. 1, no. 7, Sep. 2012. DOI: not available

[6] J. R. R. A. Martins, "Aerodynamic design optimization: Challenges and perspectives," *Comput. Fluids*, vol. 239, pp. 100–112, 2024. DOI: 10.1016/j.compfluid.2022.105479

[7] B. C. Mathewa *et al.*, "Computational study for improvement of aerodynamic performance of airfoil by changing various aerodynamic properties," *Workshop on Control and Embedded Systems*, 2021.

[8] H. Pandeya, D. Fernandes, A. Khandelwal, and D. Mishrab, "Finite element analysis of fatigue and fracture behavior in idealized airplane wing model with embedded crack under wind load," *IOP Conf. Ser.: Earth Environ. Sci.*, vol. 796, Art. no. 012043, 2021. DOI: 10.1088/1755-1315/796/1/012043

[9] S. M. Shohel, N. Kumara, N. Bihala, and M. Mehtaa, "A comparative study of finite element analysis on cantilever beam with different materials subjected to uniformly distributed load," *NeuroQuantology*, vol. 20, no. 9, pp. 2230–2236, 2022. DOI: 10.14704/nq.2022.20.9.NQ22956

[10] R. Abdel-Rahman and B. S. Eldin, *Engineering Solid Mechanics*. CRC Press, 1999.

[11] M. Janssen, J. Zuidema, and R. J. H. Wanhill, *Fracture Mechanics*, 2nd ed.

[12] F. A. Al-Shamma, "The effect of fatigue on crack propagation in flat plates under buckling, bending and shear," *Jordan J. Mech. Ind. Eng.*, vol. 3, no. 4, pp. 206–215, 2009.

[13] F. A. Lowenheim, *Modern Electroplating*, 2nd ed.

[14] D. F. Socie and G. B. Marquis, *Multiaxial Fatigue Handbook*. Society of Automotive Engineers, Warrendale, PA, 2000.

[15] F. A. Al-Shamma and O. A. Jassim, "Dynamic crack propagation in nano-composite thin plates under multi-axial cyclic loading," *J. Mater. Res. Technol.*, vol. 8, pp. 4672–4681, 2019. DOI: 10.1016/j.jmrt.2019.07.025